MicroRNA-130a-3p promotes the proliferation and inhibits the apoptosis of cervical cancer cells via negative regulation of RUNX3

MENG WANG[1*], XIAOXIA WANG[1*] and WENFENG LIU[2]

[1]Department of Gynecology, Changle County People's Hospital, Weifang, Shandong 262400;
[2]Department of Gynecology, Jinan People's Hospital, Laiwu, Shandong 271100, P.R. China

Received December 19, 2019; Accepted June 15, 2020

DOI: 10.3892/mmr.2020.11368

Abstract. Aberrant expression of microRNAs (miRs) has been reported in various types of cancer. The aim of the present study was to investigate the role and underlying molecular mechanism of miR-130a-3p in cervical cancer (CC). The expression of miR-130a-3p in CC tissues and cell lines (CaSki and SiHa) was measured via reverse transcription-quantitative PCR. SiHa and CaSki cells were transfected with miR-130a-3p mimics and a miR-130a-3p inhibitor, respectively. The proliferation, apoptosis and migration and invasion abilities of CC cells were then measured using MTT, flow cytometry, wound-healing and Transwell assays, respectively. TargetScan and dual-luciferase reporter gene assays were performed to analyze the association between miR-130a-3p and its predicted target gene Runt-related transcription factor 3 (RUNX3). In addition, a xenograft tumor model was established in mice to evaluate the impact of miR-130a-3p on tumor growth *in vivo*. The expression of miR-130a-3p was markedly upregulated in CC tissues and cell lines compared with normal tissues and cells. Transfection with miR-130a-3p mimics significantly promoted the proliferation, migration and invasion, and inhibited the apoptosis of SiHa cells. Treatment of CaSki cells with a miR-130a-3p inhibitor resulted in opposite effects to those of miR-130a-3p mimics. RUNX3 was identified as the target gene of miR-130a-3p, and overexpression of RUNX3 eliminated the tumor-promoting effect of miR-130a-3p mimics on CC cells. Overexpression of miR-130a-3p also promoted tumor growth in mice. In conclusion, miR-130a-3p promoted proliferation, migration and invasion, and inhibited the apoptosis of CC cells via targeting RUNX3, suggesting a novel treatment target for CC.

Correspondence to: Dr Meng Wang, Department of Gynecology, Changle County People's Hospital, 278 Limin Street, Changle County, Weifang, Shandong 262400, P.R. China
E-mail: wangmeng1680@126.com

*Contributed equally

Key words: microRNA-130a-3p, RUNX3, proliferation, apoptosis, cervical cancer

Introduction

Cervical cancer (CC) frequently occurs in women over the age of 15 years and is the second leading cause of cancer-associated mortality (1). Although the morbidity and mortality rates of CC have been decreasing over the past 30 years, the 5-year survival rate of patients with CC at an advanced stage remains <40% (2,3). At present, the treatments for patients with CC primarily include surgery, radiotherapy and chemotherapy (4). Despite their wide application in clinical practice, the outcome remains unsatisfactory, which is mainly due to the metastasis of CC (5). Therefore, there is an urgent need to search for effective therapeutic strategies by exploring the mechanisms underlying CC.

MicroRNAs (miRNAs/miRs) are a class of small RNA molecules 21-25 nucleotides in length, which serve important roles in several biological processes, such as cell proliferation, migration, invasion and tumorigenesis via regulating specific target genes (6-8). Abnormal dysregulation of miRNAs and their targets has also been associated with the development of CC. For example, miR-106a has been reported to enhance cell migration and invasion, and increased matrix metalloproteinase expression in CC cells via targeting TIMP metallopeptidase inhibitor 2 (TIMP2) (9). In addition, miR-149 has been suggested to inhibit the proliferation and promote the apoptosis of CC cells via targeting GIT1 (10). miR-130a has emerged as an important miRNA in the development and progression of numerous types of malignancy, including hepatocellular carcinoma (HCC), ovarian cancer, glioblastoma, prostate carcinoma and CC (11). Kong *et al* (12) demonstrated that miR-130a-3p may be a therapeutic target for breast cancer. Liu *et al* (13) further suggested that upregulation of miR-130a-3p expression suppressed the migration and invasion of HCC cells through downregulating expression of its target gene SMAD4. However, the biological function of miR-130a-3p in CC remains unclear.

Runt-related transcription factor 3 (RUNX3) is located at chromosome 1p.13-p36.11, and has been demonstrated to have an anti-tumor role in numerous types of cancer (14). Huang *et al* (15) revealed that RUNX3 exerted a tumor-inhibiting effect on breast cancer via modulating estrogen receptor-α. RUNX3 has also been reported to inhibit the tumorigenesis of HCC by suppressing cancer stem cells in a jagged 1-mediated manner (16). RUNX3 may also have a major

role in the cellular processes of tumorigenesis and metastasis, including epithelial-mesenchymal transition (EMT) (17), adhesion (18), invasion (19) and apoptosis (20). Zhen *et al* (21) revealed that overexpression of RUNX3 suppressed the proliferation, migration and invasion of CC cells, thus suggesting that RUNX3 may function as a tumor suppressor in CC. However, the regulatory relationship between miR-130a-3p and RUNX3 in CC remains unclear.

In the present study, the expression of miR-130a-3p was evaluated in both CC tissues and cell lines. Functional experiments were performed to analyze the regulatory role of miR-130a-3p in CC *in vitro*, and *in vivo* using a mouse xenograft model. Furthermore, the target genes of miR-130a-3p were assessed with a focus on the association with RUNX3 in the CC models. The findings of the present study highlighted miR-130a-3p as a promising biomarker and therapeutic target for CC.

Materials and methods

Clinical specimens. A total of 50 paired CC tissues and adjacent normal tissues (within 5 cm of the tumors) were obtained from patients with CC (age range, 35-66 years; mean age, 46.1±4.9 years) via surgical resection from April 2017 to July 2018 at Changle County People's Hospital (Weifang, China). All CC tissues were confirmed via histopathological examination. The inclusion criterion was first-time diagnosis. The exclusion criteria included the presence of other types of malignant tumor and patients who had received CC treatment before admission. The clinicopathological features of the patients were recorded, including age, tumor size, tumor grade, Federation of Gynecology and Obstetrics (FIGO) stage (22), lymphatic metastasis and depth of cervical invasion. Informed, written consent was obtained from all patients, and the study received approval from the ethics committee of Changle County People's Hospital (approval no. 2016013; Weifang, China).

Cell lines and culture. Normal human cervical epithelial cells (Ect1/E6E7) and CC cell lines (CaSki and SiHa) were purchased from The Cell Bank of Type Culture Collection of the Chinese Academy of Sciences. The cells were cultured in RPMI-1640 medium (HyClone; GE Healthcare life Sciences) supplemented with 10% FBS (HyClone; GE Healthcare life Sciences) in an incubator (MCO-15AC; SANYO Electric Co., Ltd.) at 37˚C and 5% CO_2 with saturated humidity.

Reverse transcription-quantitative PCR (RT-qPCR). Total RNA was extracted from the tissues and cells using TRIzol® Plus RNA Isolation reagents (Invitrogen; Thermo Fisher Scientific, Inc.). RNA (1 μg) was reverse transcribed into cDNA at 42˚C for 45 min using a miScript II RT kit (Qiagen GmbH). The qPCR reaction was performed using an ABI 7500HT Fast Real-Time PCR system (Applied Biosystems; Thermo Fisher Scientific, Inc.) with SYBRGreen master mix (CoWin Biosciences). The reaction conditions were as follows: 95˚C for 3 min, followed by 40 cycles at 95˚C for 15 sec and 60˚C for 30 sec, and a final extension step at 72˚C for 1 min. The mRNA/miRNA expression levels were calculated using the $2^{-\Delta\Delta Cq}$ method (23). The primer sequences are listed in Table I. U6 or β-actin was used as the internal reference for detection of miR-130a-3p or RUNX3, respectively.

Cell transfection. When SiHa or CaSki cells reached 80% confluence, they were seeded into 6-well cell culture plates ($6x10^5$ cells/well). miR-130a-3p mimics (cat. no. B01001), miR-130a-3p inhibitor (cat. no. B03001) and corresponding negative controls [NCs; mimics-NC (cat. no. B04004) and inhibitor-NC (cat. no. B04006)] were synthesized by Shanghai GenePharma Co., Ltd. miR-130a-3p mimics or mimics-NC (20 nM) were transfected into SiHa cells, and miR-130a-3p inhibitor or inhibitor-NC (20 nM) were transfected into CaSki cells using Lipofectamine® 2000 (Invitrogen; Thermo Fisher Scientific, Inc.). Cells without transfection were considered as the mock group. In addition, pcDNA3.1-RUNX3 (pcDNA3.1, carrying the RUNX3 coding sequence) and pcDNA3.1-NC (empty vector), synthesized by Sangon Biotech Co., Ltd., were co-transfected in SiHa cells (20 nM) with miR-130a-3p mimics/mimics-NC (20 nM) using Lipofectamine® 2000. After transfection for 48 h at 37˚C, the cells were collected for follow-up experiments.

Dual-luciferase reporter gene assay. TargetScan release 5.2 (http://www.targetscan.org) was used to predict the presence of a binding site for miR-130-3p on the RUNX3 sequence. Based on this prediction, the 3'-untranslated region (UTR) of RUNX3 containing wild-type (Wt) or mutated (Mut) binding sites were synthesized by Shanghai GenePharma Co., Ltd., and were then inserted into the PsiCHECK-2 vector (Promega Corporation) to obtain RUNX3-Wt and RUNX3-Mut, respectively. SiHa cells ($2x10^5$ cells/well) were co-transfected with RUNX3-Mut/RUNX3-Wt and miR-130a-3p mimics/mimics-NC (Shanghai GenePharma Co., Ltd.) using Lipofectamine® 2000. Following 48 h of incubation at 37˚C, *Renilla* and firefly luciferase activities were detected using a Dual-Luciferase Reporter assay system (Promega Corporation), according to the manufacturer's protocol. Firefly luciferase activity was normalized to *Renilla* luciferase activity.

Western blotting. Total proteins were extracted from SiHa or CaSki cells using RIPA lysis buffer (Beyotime Institute of Biotechnology) and quantified using a Bicinchoninic Acid Protein Assay kit (Thermo Fisher Scientific, Inc.). The protein samples (40 μg) were separated by sodium dodecyl sulfate-polyacrylamide gel electrophoresis on 10% gels and electroblotted onto a polyvinylidene fluoride membrane. The membrane was blocked with 5% skim milk in Tris-buffered saline containing 0.1% Tween 20 (TBST) for 1 h at room temperature and incubated with anti-GAPDH (1:1,000; cat. no. ab9485; Abcam) and anti-RUNX3 (1:1,000; cat. no. ab224641; Abcam) antibodies at 4˚C overnight. After three washes with TBST, the membrane was incubated with a horseradish peroxidase-conjugated goat anti-rabbit IgG secondary antibody (1:10,000; cat. no. 7074; Cell Signaling Technology, Inc.) for 1 h at 25˚C. Protein bands were visualized using a chemiluminescent substrate kit (Invitrogen; Thermo Fisher Scientific, Inc.) and analyzed using Gel-Pro Analyzer software (version 4.0; Media Cybernetics, Inc.). GAPDH was used as the internal reference.

Table I. Primer sequences.

Name of primer	Sequences
miR-130a-3p	Forward: 5'-GATGCTCTCAGTGCAATGTTA-3'
	Reverse: 5'-CTCTGTCTCTCGTCTTGTTGGTAT-3'
U6	Forward: 5'-CTCGCTTCGGCAGCACA-3'
	Reverse: 5'-AACGCTTCACGAATTTGCGT-3'
RUNX3	Forward: 5'-TCTGTAAGGCCCAAAGTGGGTA-3'
	Reverse: 5'-ACCTCAGCATGACAATATGTCACAA-3'
β-actin	Forward: 5'-ACACCTTCTACAATGAGCTG-3'
	Reverse: 5'-CTGCTTGCTGATCCACATCT-3'

RUNX3, Runt-related transcription factor 3; miR, microRNA.

MTT assay. Cells were seeded into 96-well plates ($6x10^3$ cells/well, 200 μl/well) and were incubated at 37˚C. At 0, 24, 48 and 72 h of culture, 20 μl MTT reagent (5 mg/ml; Sigma-Aldrich; Merck KGaA) was added to each well. After 4 h of incubation at 37˚C, 150 μl dimethyl sulfoxide was added to terminate the reaction. The optical density at 450 nm (OD_{450}) was detected using a microplate reader (Applied Biosystems; Thermo Fisher Scientific, Inc.). The growth curves were drawn as a plot of the OD value over time. This experiment was performed in triplicate and was repeated three times.

Annexin V-propidium iodide (PI) double staining assay. To detect the early apoptosis of CC cells resulting from the various treatments, cells ($1x10^5$) were suspended in 500 μl binding buffer and then stained with 5 μl Annexin V-enhanced green-fluorescent protein and 5 ml PI using the eBioscience™ Annexin V-FITC apoptosis detection kit (Invitrogen; Thermo Fisher Scientific, Inc.) at 25˚C for 10 min in the dark. Subsequently, apoptosis was detected using a FACScan flow cytometer (version 2.0; BD Biosciences) and the data were analyzed using CellQuest version 5.1 software (BD Biosciences).

Wound-healing assay. Cells were seeded into 6-well plates ($1x10^6$/well). When cells reached 90% confluence, a scratch was created using a 10-μl pipette tip. After 48 h of culturing in serum-free medium, the wound gaps were observed under an inverted light microscope (magnification, x200) and measured using ImageJ software (version 1.46; National Institutes of Health). The relative migration rate was calculated as (original gap distance-gap distance at 48 h)/original gap distance x100 and normalized to that of the mock group. This experiment was performed in triplicate and was repeated three times.

Transwell invasion assay. The upper chamber of Transwell inserts was precoated at 37˚C for 30 min with Matrigel (BD Biosciences) according to the manufacturer's instructions 1 day before the experiment. The cells ($1x10^6$) were resuspended in serum-free medium and then transferred onto the Matrigel-coated upper chamber, and RPMI 1640 containing 10% FBS was added to the lower chamber. After incubation for 24 h at 37˚C, the non-invaded cells in the upper chamber were scraped off with cotton swabs, and the cells that invaded the lower inserts were fixed with 90% ethanol and stained with Coomassie brilliant blue at 37˚C for 30 min. The stained cells were imaged and counted in five random fields under an inverted light microscope (magnification, x200). The number of invading cells was calculated by normalizing to that of the mock group. This experiment was performed in triplicate and was repeated three times.

Xenograft tumor mouse model. All experimental procedures with mice were performed according to the Chinese legislation regarding research with experimental animals. The animal study received approval from the Ethics Committee of Changle County People's Hospital (approval no. 2016013). The healthy male BALB/c nude mice (weight, 20±2 g; age, 4 weeks; n=15) were obtained from Shanghai Experimental Animal Center of Chinese Academy of Sciences. The animals were housed in a sterile environment at a controlled temperature of 20˚C and 40% relative humidity, under a 12-h light/dark cycle with free access to food and water. Subsequently, the mice were randomly divided into three groups: Mock, mimics-NC and miR-130a-3p mimics (n=5/group). The mock and transfected SiHa cells at the logarithmic growth phase ($1x10^7$ cells/nude mice, 200 μl) were resuspended in PBS and injected into the intradermal left axilla of the mice. The longest diameter (L) and the shortest diameter (W) of the xenograft tumors were measured with a Vernier caliper every 7 days after injection, and the tumor volume was calculated using the following formula: $V=L \times W^2/2$. At the end of week 4, the mice were anesthetized by an intraperitoneal injection of 50 mg/kg pentobarbital sodium and were then sacrificed by cervical dislocation. The xenograft tumors were dissected completely and weighed.

Statistical analysis. Statistical analysis was performed using SPSS 22.0 statistical software (IBM Corp.) and Prism v7.01 (GraphPad Software, Inc.). Data are presented as the mean ± standard deviation. A paired Student's t-test was used to compare differences between two groups. One-way analysis of variance followed by Tukey's post-hoc test was applied for analyzing more than two groups. Differences in clinicopathological features between patients with CC with high or low expression of miR-130a-3p were determined by χ^2 test (group size >5) or Fisher's exact test (group size ≤5). Pearson's correlation analysis was used to determine the correlation

Table II. Association between miR-130a-3p expression and clinicopathological features of patients with cervical cancer.

Clinicopathological features	Total no. of cases	High miR-130a-3p (n=17)	Low miR-130a-3p (n=23)	P-value
Age (years)				0.45
<55	23	9	14	
≥55	17	8	9	
Tumor size (cm)				0.08
<4	18	5	13	
≥4	22	12	10	
Tumor grade				0.21
G1/G2	20	7	13	
G3	20	10	10	
FIGO stage				0.003[a]
I/II	23	4	19	
III/IV	17	13	4	
Lymph node metastasis				0.0009[a]
No	24	5	19	
Yes	16	12	4	
Depth of cervical invasion (mm)				0.0244[a]
<2/3	25	7	17	
≥2/3	15	10	6	

The difference between high and low groups was determined by χ^2 test (group size >5) or Fisher's exact test (group size ≤5); [a]P<0.05. FIGO, Federation of Gynecology and Obstetrics; miR, microRNA.

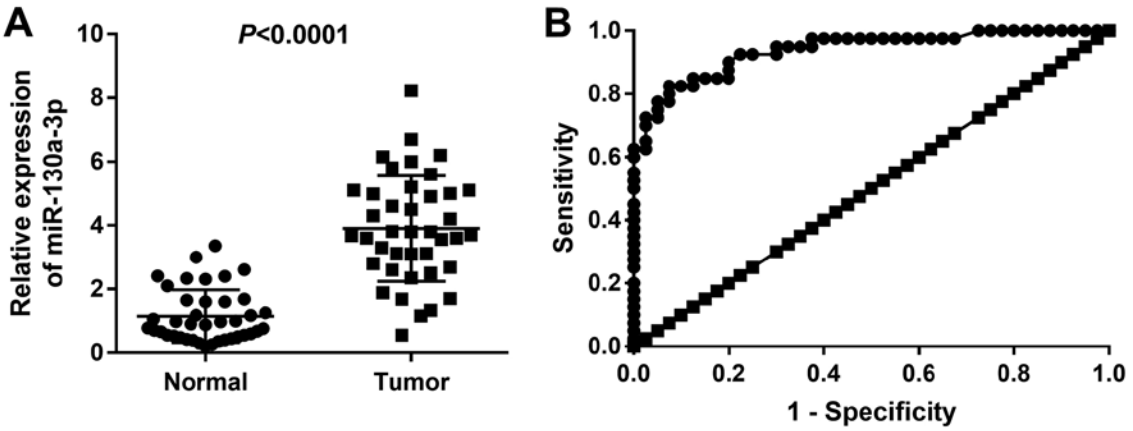

Figure 1. miR-130a-3p expression is upregulated in CC tissues. (A) RT-qPCR was used to measure the relative expression levels of miR-130a-3p in patients with CC (n=40). (B) Receiver operating characteristic curve was used to evaluate the diagnostic value of miR-130a-3p in CC. CC, cervical cancer; miR, microRNA.

between the expression levels of miR-130a-3p and RUNX3 in CC tissues. The diagnostic analysis was performed through receiver operating characteristic (ROC) curve analysis with healthy controls as true negative cases and patients with CC as true positive cases. All experiments were conducted in triplicate, with ≥3 independent experiments. P<0.05 was considered to indicate a statistically significant difference.

Results

miR-130a-3p expression is upregulated in CC. The expression levels of miR-130a-3p were significantly higher in the tumor tissues compared with in the normal tissues of patients with CC (P<0.0001; Fig. 1A). Patients with CC were then divided into two groups (high and low expression) according to the median miR-130a-3p expression levels (3.901). As indicated in Table II, high expression of miR-130a-3p in patients with CC exhibited strong associations with FIGO stage (P=0.003), lymph node metastasis (P=0.0009) and depth of cervical invasion (P=0.0244), but not with age, tumor size or tumor grade. The area under the ROC curve value for discriminating between CC and normal tissues was 0.938 (95% confidence interval, 0.888-0.988), and the sensitivity and specificity were 82.5 and 92.5%, respectively (Fig. 1B).

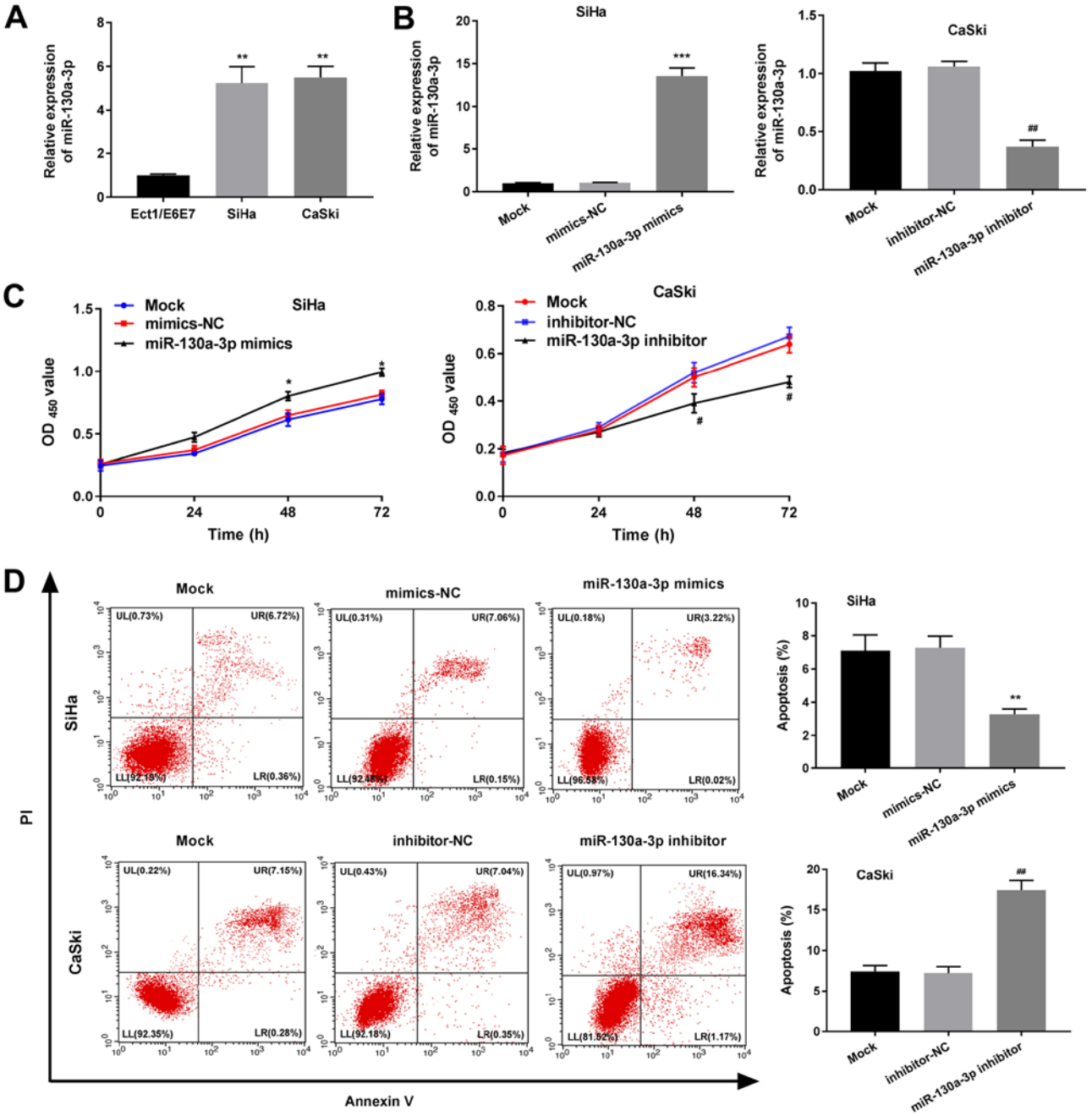

Figure 2. miR-130a-3p promotes the proliferation and inhibits the apoptosis of CC cells. (A) Relative expression of miR-130a-3p in CC cell lines determined by RT-qPCR. **P<0.01 vs. Ect1/E6E7. (B) Efficiency of transfection assessed by RT-qPCR. (C) OD_{450} value of SiHa and CaSki cells detected by MTT assays. (D) Flow cytometry was used to detect the apoptosis of SiHa and CaSki cells. **P<0.01, ***P<0.001 vs. mimics-NC; ##P<0.01 vs. inhibitor-NC;. CC, cervical cancer; miR, microRNA; RT-qPCR, reverse transcription-quantitative PCR; OD, optical density; NC, negative control; PI, propidium iodide.

miR-130a-3p enhances the proliferation and suppresses the apoptosis of CC cells. As revealed in Fig. 2A, the expression levels of miR-130-3p were significantly higher in CaSki and SiHa cells than in normal cervical epithelial cells (Ect1/E6E7) (P<0.01). RT-qPCR further revealed that the expression levels of miR-130-3p were significantly elevated in the miR-130a-3p mimics group compared with in the mimics-NC group (P<0.001; Fig. 2B). The proliferation detected via MTT analysis was also significantly increased in the miR-130a-3p mimics group compared with that in the mimics-NC group (P<0.05; Fig. 2C). As demonstrated in Fig. 2D, apoptosis of the miR-130a-3p mimics group was significantly reduced compared with that of the mimics-NC group (P<0.01). All of the effects observed in the miR-130-3p mimics group were the opposite of those observed in the miR-130a-3p inhibitor group.

miR-130a-3p promotes the migration and invasion abilities of CC cells. As demonstrated in Fig. 3A, the relative migration rate of cells in the miR-130a-3p mimics group was significantly enhanced compared with that of the cells in the mimics-NC group (P<0.01). The relative number of invasive cells was also significantly enhanced in the miR-130a-3p mimics group compared with that in the mimics-NC group (P<0.01; Fig. 3B). The opposite effects were observed in the

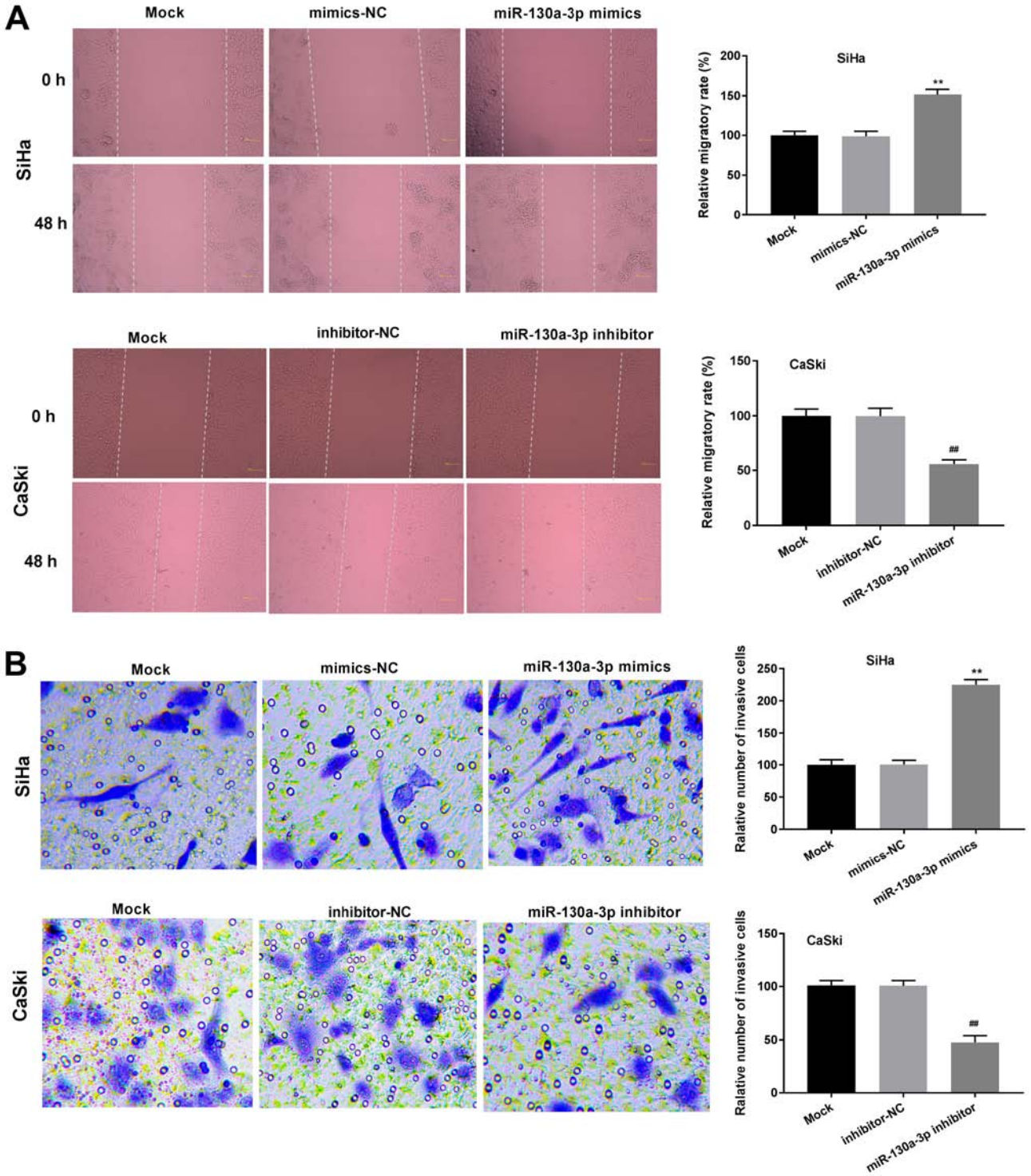

Figure 3. miR-130a-3p promotes the migration and invasion abilities of cervical cancer cells. (A) Wound-healing assays were used to assess the relative migration rate of SiHa and CaSki cells. Magnification, x200. (B) Number of invasive cells was detected by a Transwell assay. Magnification, x200. **P<0.01 vs. mimics-NC; $^{\#\#}$P<0.01 vs. inhibitor-NC. miR, microRNA; NC, negative control.

miR-130-3p inhibitor group. Transfection with mimics-NC or inhibitor-NC did not affect the relative migration rate or relative number of invasive cells.

RUNX3 is a target gene of miR-130a-3p. As shown in Fig. 4A, the relative mRNA expression levels of RUNX3 were reduced in CC tissues compared with in normal tissues (P<0.0001). Pearson's correlation analysis revealed a negative correlation between the expression levels of miR-130a-3p and RUNX3 in CC tissues (r=-0.57; P=0.0001; Fig. 4B). Consistently, compared with in normal Ect1/E6E7 cells, the mRNA expression levels of RUNX3 were significantly reduced in CaSki and SiHa CC cells (P<0.01; Fig. 4C).

TargetScan predicted a binding site for miR-130a-3p at the 3'-UTR of RUNX3 (Fig. 4D). The miR-130a-3p mimics significantly decreased the luciferase activity of RUNX3-Wt

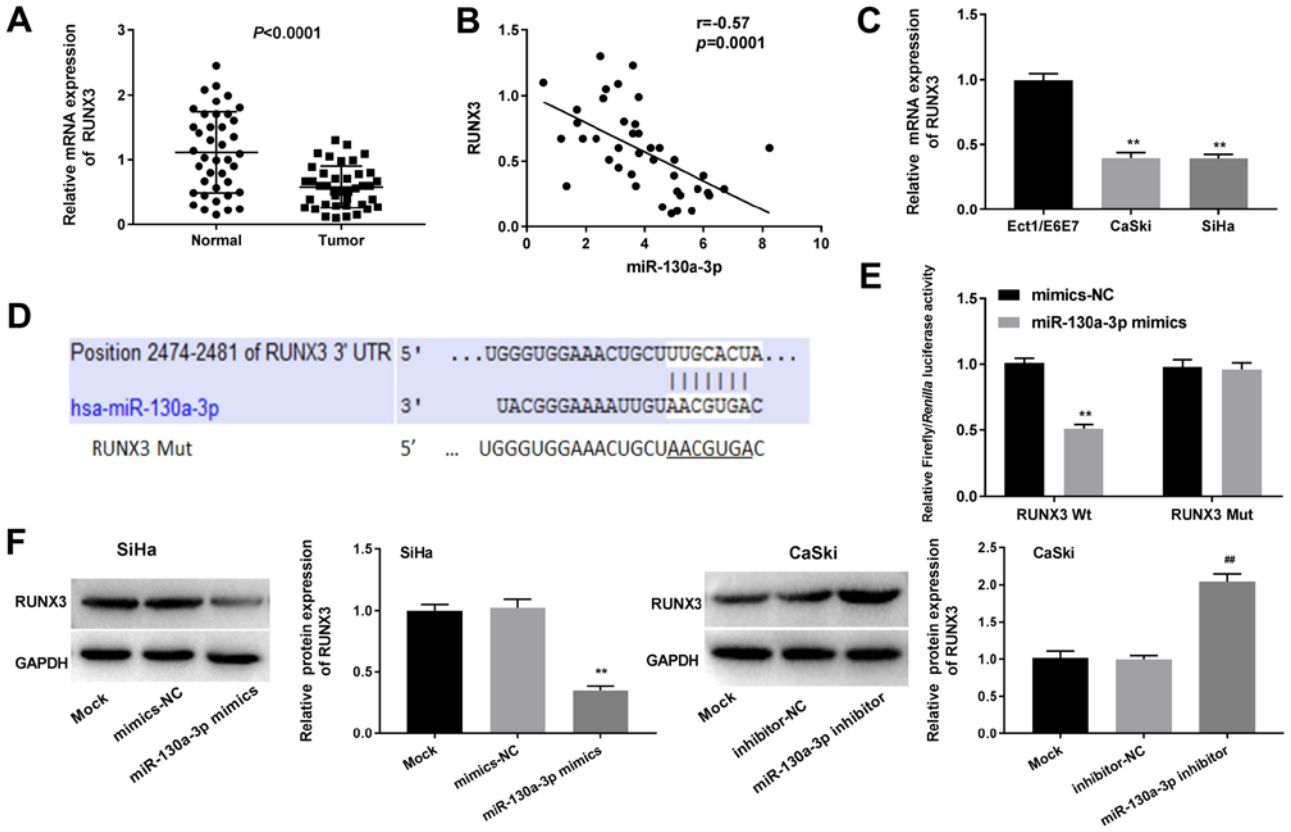

Figure 4. miR-130a-3p directly targets RUNX3. (A) Relative mRNA expression levels of RUNX3 in CC tissues, as determined by RT-qPCR. (B) Pearson's correlation analysis was used to detect the correlation between the expression levels of miR-130a-3p and RUNX3. (C) Relative mRNA expression levels of RUNX3 in CC cell lines, as determined by RT-qPCR. **P<0.01 vs. Ect1/E6E7. (D) TargetScan was used to predict the binding site between RUNX3 and miR-130a-3p. (E) Dual-luciferase reporter gene assays were used to detect the luciferase activity of SiHa cells co-transfected with miR-130a-3p mimics or mimics-NC, and RUNX3-Wt or RUNX3-Mut. **P<0.01 vs. mimics-NC. (F) Relative protein expression of RUNX3, as determined via western blotting. $^{\#\#}$P<0.01 vs. inhibitor-NC; **P<0.01 vs. mimics-NC. RUNX3, Runt-related transcription factor 3; CC, cervical cancer; miR, microRNA; RT-qPCR, reverse transcription-quantitative PCR; NC, negative control; Wt, wild-type; Mut, mutated.

compared with the mimics-NC, but did not influence the luciferase activity of RUNX3-Mut (P<0.01; Fig. 4E). As indicated in Fig. 4F, the relative protein expression of RUNX3 was significantly downregulated by miR-130a-3p upregulation and upregulated by miR-130a-3p downregulation compared with the mimics-NC groups (P<0.01). Transfection with mimics-NC or inhibitor-NC did not influence the luciferase activity or relative protein expression of RUNX3. These findings suggested that RUNX3 may represent a target gene of miR-130a-3p.

RUNX3 eliminates the tumor-promoting effects of miR-130a-3p on CC cells. Western blot analysis revealed that the relative protein expression of RUNX3 was significantly enhanced in the pcDNA3.1-RUNX3 group compared with that in the pcDNA3.1-NC group (P<0.01). However, transfection with pcDNA3.1-NC did not influence the relative protein expression of RUNX3 (Fig. 5A). In addition, the OD_{450} value, relative migration rate and relative number of invasive cells were significantly increased in the pcDNA3.1-NC + miR-130a-3p mimics group, and were significantly decreased in the RUNX3 + mimics-NC group compared with those in the pcDNA3.1-NC + mimics-NC group (P<0.05; Fig. 5B, D and E). However, the overexpression of RUNX3 reversed the promoting effects of miR-130a-3p mimics on the proliferation, migration and invasion of SiHa cells. The results of the double staining assay for apoptosis revealed the opposite pattern to those of the MTT assay (P<0.05; Fig. 5C).

miR-130a-3p promotes tumor growth in nude mice. To confirm the effect of miR-130a-3p on CC tumorigenesis, SiHa cells transfected with mimics-NC or miR-130a-3p mimics were injected into the intradermal left axilla of nude mice. As shown in Fig. 6A and B, the tumor volume and weight were significantly increased in the miR-130a-3p mimics group compared with in the mimics-NC group (P<0.05). Moreover, the relative expression levels of miR-130a-3p in tumor xenograft tissues were elevated in the miR-130a-3p mimics group in comparison with those in the mimics-NC group (P<0.001; Fig. 6C), whereas the relative mRNA expression levels of RUNX3 were significantly reduced in the miR-130a-3p mimics group in comparison with those in the mimics-NC group (P<0.01; Fig. 6D).

Discussion

miRNAs function as oncogenes or anti-tumor genes and serve critical roles in tumor progression (10). Numerous oncomiRs have been discovered in CC to date, including miR-21 (24), miR-10a (25) and miR-133b (26). In the present study, it

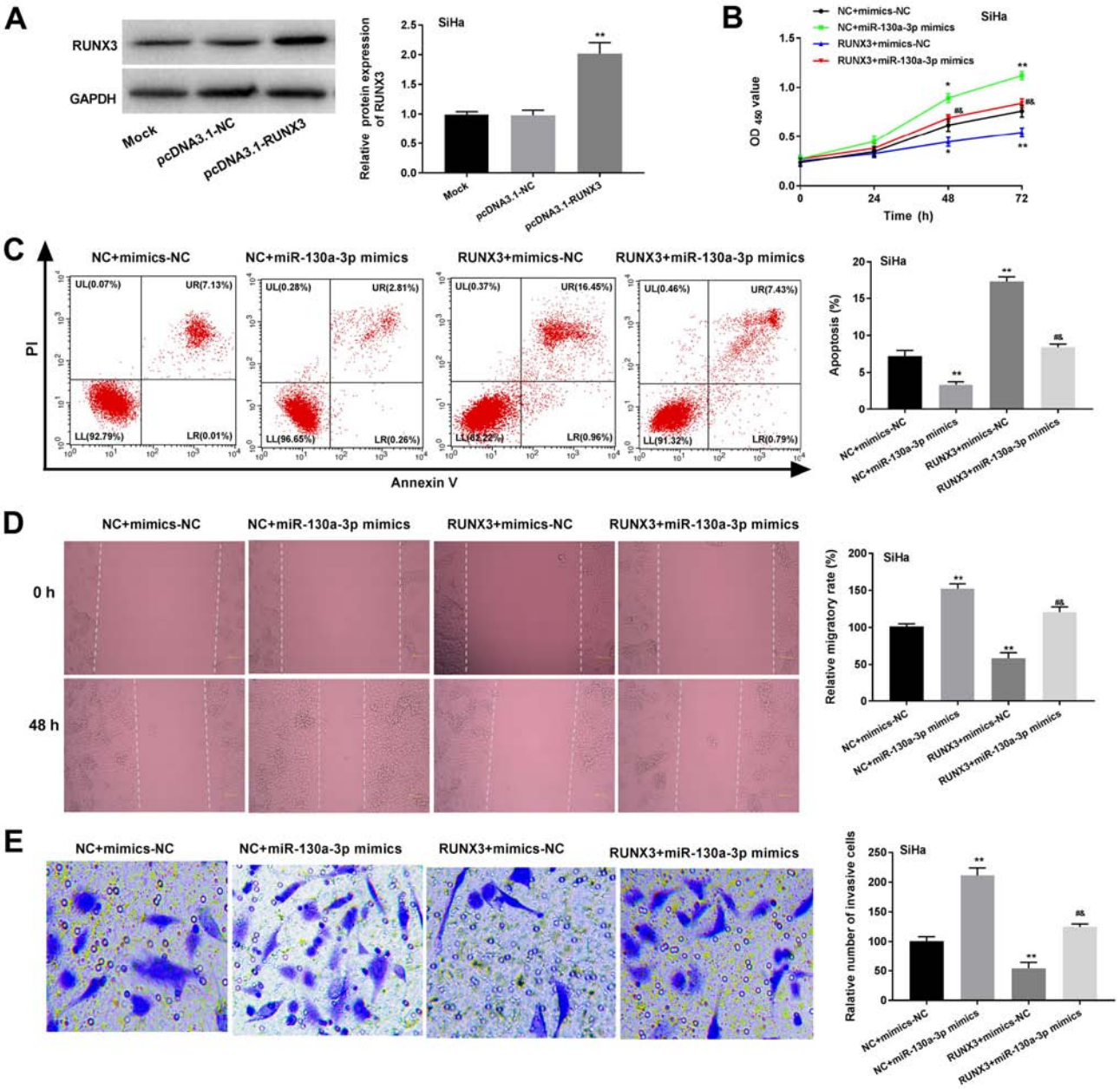

Figure 5. RUNX3 overexpression eliminates the effects of miR-130a-3p on cervical cancer. (A) Western blotting was performed to assess the overexpression efficiency of RUNX3 in pcDNA3.1-RUNX3-transfected SiHa cells. **P<0.01 vs. pcDNA3.1-NC. (B) MTT assays were used to detect the OD_{450} value of SiHa cells. (C) Apoptosis of SiHa was examined using flow cytometry. (D) Relative migration rate was analyzed by wound-healing assays. Magnification, x200. (E) Number of invasive cells was assessed by Transwell assays. Magnification, x200. *P<0.05, **P<0.01 vs. NC + mimics-NC; $^{\#}$P<0.05 vs. NC + miR-130a-3p mimics; $^{\&}$P<0.05 vs. RUNX3 + mimics-NC. RUNX3, Runt-related transcription factor 3; miR, microRNA; NC, negative control; OD, optical density.

was revealed that the expression levels of miR-130a-3p were significantly increased in CC tissues compared with in adjacent normal tissues, indicating that miR-130a-3p may be an oncogene in CC. Abnormal expression of miR-130a has been reported to be closely associated with tumor progression. Chen *et al* (27) reported that upregulation of miR-130a expression was associated with the TNM stage and lymph node metastasis of colorectal cancer. Yin *et al* (28) demonstrated that upregulation of miR-130a was significantly associated with lymph node metastasis and an advanced clinical stage of CC. Consistent with these previous studies, the present study demonstrated that high expression of miR-130a-3p was significantly associated with the FIGO stage, lymph node metastasis and depth of cervical invasion in patients with CC. These findings further support that miR-130a-3p may act as a tumor promoter in CC. It was therefore hypothesized that the upregulation of miR-130a-3p expression may have clinical value in the prediction of CC. This hypothesis was supported by the ROC curve revealing the diagnostic value of miR-130a-3p for CC. The current findings demonstrated that miR-130a-3p may be a potential biomarker for the diagnosis and prognosis of CC.

To further confirm the oncogenic effect of miR-130a-3p on CC, a series of functional experiments were performed to identify the regulatory role of miR-130a-3p on CC cells. As expected, it was demonstrated that overexpression of

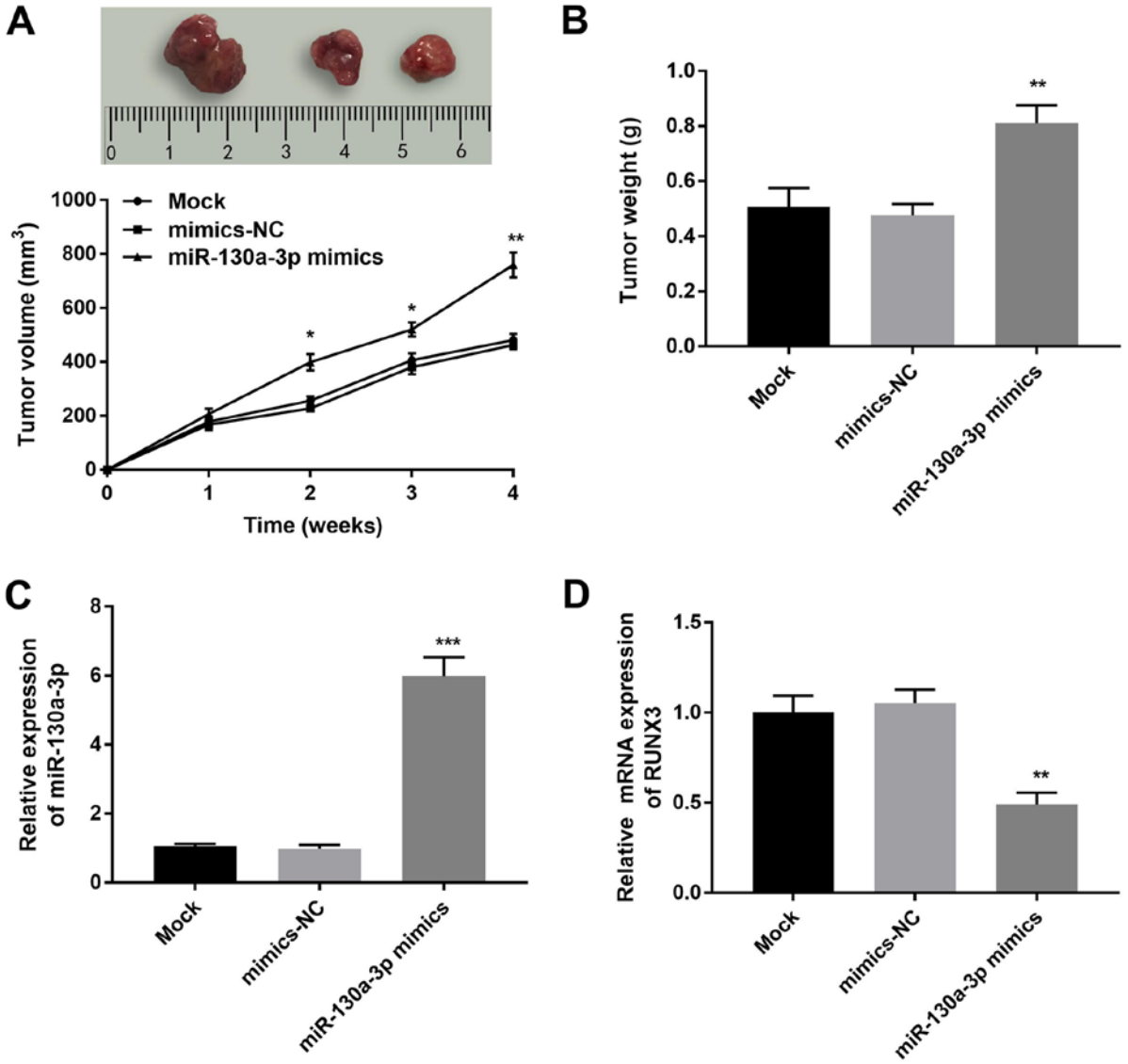

Figure 6. miR-130a-3p promotes tumor growth in mice. (A) Tumor morphology at week 4 and tumor volume at different time points. (B) Tumor weight in mice at week 4. Reverse transcription-quantitative PCR was used to examine the relative mRNA expression levels of (C) miR-130a-3p and (D) RUNX3 in tumors. *P<0.05, **P<0.01, ***P<0.001 vs. mimics-NC. RUNX3, Runt-related transcription factor 3; NC, negative control; miR, microRNA.

miR-130a-3p enhanced the proliferation, migration and invasiveness, and inhibited the apoptosis of CC cells. A previous study demonstrated that the miR-130 family (miR-130b, miR-301a and miR-301b) promoted the migration and invasion of bladder cancer cells via negative regulation of phosphatase and tensin homolog (PTEN) (18). Jiang *et al* (29) revealed that miR-130a promoted the proliferation, migration and invasion of gastric cancer cells via targeting RUNX3, and Yin *et al* (28) verified that miR-130a enhanced the proliferation and invasion of CC cells via modulating TIMP2. In accordance with the results of these previous studies, in the present study it was concluded that the upregulation of miR-130a-3p contributed to the progression of CC. Therefore, silencing miR-130a-3p may represent a potential therapeutic strategy for CC.

miRNAs exert their functions via regulating the expression of corresponding target genes. For example, miR-130a has been reported to enhance the migration, invasion and EMT of osteosarcoma cells through suppressing PTEN (30). miR-130a may also promote cell proliferation, migration and invasion via targeting RUNX3 in gastric cancer (29). In the present study, RUNX3 was identified as a target gene of miR-130a-3p. Supporting this result, a negative correlation was observed between the expression levels of miR-130a-3p and RUNX3 in CC tissues. RUNX3 is mapped on human chromosome 1p36, and has been reported to serve as an anti-tumor gene in lung (31), bladder (32) and gastric cancer (33). Li *et al* (21) revealed that knockdown of RUNX3 promoted the proliferation, migration and invasiveness of CC cells. Similarly, Gao *et al* (34) reported that upregulation of RUNX3 inhibited the proliferation of CC cells. Consistent with these previous studies, it was demonstrated in the present study that the expression levels of RUNX3 were significantly decreased in CC cell lines. Moreover, RUNX3 overexpression eliminated the tumor-promoting effects of miR-130a-3p on the proliferation, migration, invasiveness and apoptosis of CC cells. These results indicated that miR-130a-3p may promote the tumorigenesis of CC through targeting RUNX3. The present *in vivo* assay further confirmed this hypothesis.

RUNX3 can also be regulated by promoter methylation (35). Aberrant methylation of CpG islands of RUNX3 has been demonstrated to reduce the expression levels of RUNX3 in a variety of human malignancies (36-38). However, in the present study, the methylation status of RUNX3 in CC tissues, cells or xenografts was not analyzed; this will be considered in our future work.

In conclusion, miR-130a-3p was highly expressed in CC tissues and cells, and exhibited high diagnostic value. miR-130a-3p promoted the proliferation, migration and invasiveness, and inhibited the apoptosis of CC cells through targeting RUNX3. The results of the present study proposed miR-130a-3p as a promising therapeutic target for the treatment of CC and provided new research directions to further understand the pathogenesis of CC.

Acknowledgements

Not applicable.

Funding

No funding was received.

Availability of data and materials

The datasets used and/or analyzed during the current study are available from the corresponding author on reasonable request.

Authors' contributions

MW made substantial contributions to the conception and design of the study; and MW, XW and WL acquired, analyzed and interpreted the data, and drafted and revised the manuscript. All authors read and approved the final manuscript.

Ethics approval and consent to participate

Informed, written consent was obtained from all patients, and the study received approval from the Ethics Committee of Changle County People's Hospital (approval no. 2016013). The animal study also received approval from the Ethics Committee of Changle County People's Hospital (approval no. 2016013).

Patient consent for publication

Not applicable.

Competing interests

The authors declare that they have no competing interests.

References

1. Krieger N, Bassett MT and Gomez SL: Breast and cervical cancer in 187 countries between 1980 and 2010. Lancet 379: 1391-1392, 2012.
2. Bosch FX and de Sanjosé S: The epidemiology of human papillomavirus infection and cervical cancer. Dis Markers 23: 213-227, 2007.
3. Bosch FX, Lorincz A, Muñoz N, Meijer CJ and Shah KV: The causal relation between human papillomavirus and cervical cancer. J Clin Pathol 55: 244-265, 2002.
4. Franco EL, Duarte-Franco E and Ferenczy A: Cervical cancer: Epidemiology, prevention and the role of human papillomavirus infection. CMAJ 164: 1017-1025, 2001.
5. Dizon DS, Mackay HJ, Thomas GM, Werner TL, Kohn EC, Hess D, Rose PG and Covens AL: State of the science in cervical cancer: Where we are today and where we need to go. Cancer 120: 2282-2288, 2014.
6. Zhu K, He Y, Xia C, Yan J, Hou J, Kong D, Yang Y and Zheng G: MicroRNA-15a inhibits proliferation and induces apoptosis in CNE1 nasopharyngeal carcinoma cells. Oncol Res 24: 145-151, 2016.
7. Zhou Y, Yang C, Wang K, Liu X and Liu Q: MicroRNA-33b inhibits the proliferation and migration of osteosarcoma cells via targeting hypoxia-inducible factor-1α. Oncol Res 25: 397-405, 2017.
8. Wang S, Hui Y, Li X and Jia Q: Silencing of lncRNA CCDC26 restrains the growth and migration of glioma cells *in vitro* and *in vivo* via targeting miR-203. Oncol Res 26: 1143-1154, 2017.
9. Li X, Zhou Q, Tao L and Yu C: MicroRNA-106a promotes cell migration and invasion by targeting tissue inhibitor of matrix metalloproteinase 2 in cervical cancer. Oncol Rep 38: 1774-1782, 2017.
10. Qian B, Zhao L, Wang X, Xu J, Teng F, Gao L and Shen R: RETRACTED: miR-149 regulates the proliferation and apoptosis of cervical cancer cells by targeting GIT1. Biomed Pharmacother 105: 1106-1116, 2018.
11. Zhang HD, Jiang LH, Sun DW, Jian L and Ji ZL: The role of miR-130a in cancer. Breast Cancer 24: 521-527, 2017.
12. Kong X, Zhang J, Li J, Shao J and Fang L: MiR-130a-3p inhibits migration and invasion by regulating RAB5B in human breast cancer stem cell-like cells. Biochem Biophys Res Commun 501: 486-493, 2018.
13. Liu Y, Li Y, Wang R, Qin S, Liu J, Su F, Yang Y, Zhao F, Wang Z and Wu Q: MiR-130a-3p regulates cell migration and invasion via inhibition of Smad4 in gemcitabine resistant hepatoma cells. J Exp Clin Cancer Res 35: 19, 2016.
14. Subramaniam MM, Chan JY, Yeoh KG, Quek T, Ito K and Salto-Tellez M: Molecular pathology of RUNX3 in human carcinogenesis. Biochim Biophys Acta 1796: 315-331, 2009.
15. Huang B, Qu Z, Ong CW, Tsang YH, Xiao G, Shapiro D, Salto-Tellez M, Ito K, Ito Y and Chen LF: RUNX3 acts as a tumor suppressor in breast cancer by targeting estrogen receptor α. Oncogene 31: 527-534, 2012.
16. Nishina S, Shiraha H, Nakanishi Y, Tanaka S, Matsubara M, Takaoka N, Uemura M, Horiguchi S, Kataoka J, Iwamuro M, *et al*: Restored expression of the tumor suppressor gene RUNX3 reduces cancer stem cells in hepatocellular carcinoma by suppressing Jagged1-Notch signaling. Oncol Rep 26: 523-531, 2011.
17. Voon DC, Wang H, Koo JK, Nguyen TA, Hor YT, Chu YS, Ito K, Fukamachi H, Chan SL, Thiery JP and Ito Y: Runx3 protects gastric epithelial cells against epithelial-mesenchymal transition-induced cellular plasticity and tumorigenicity. Stem Cells 30: 2088-2099, 2012.
18. Egawa H, Jingushi K, Hirono T, Ueda Y, Kitae K, Nakata W, Fujita K, Uemura M, Nonomura N and Tsujikawa K: The miR-130 family promotes cell migration and invasion in bladder cancer through FAK and Akt phosphorylation by regulating PTEN. Sci Rep 6: 20574, 2016.
19. Sakakura C, Hasegawa K, Miyagawa K, Nakashima S, Yoshikawa T, Kin S, Nakase Y, Yazumi S, Yamagishi H, Okanoue T, *et al*: Possible involvement of RUNX3 silencing in the peritoneal metastases of gastric cancers. Clin Cancer Res 11: 6479-6488, 2005.
20. Yano T, Ito K, Fukamachi H, Chi XZ, Wee HJ, Inoue K, Ida H, Bouillet P, Strasser A, Bae SC and Ito Y: The RUNX3 tumor suppressor upregulates Bim in gastric epithelial cells undergoing transforming growth factor beta-induced apoptosis. Mol Cell Biol 26: 4474-4488, 2006.
21. Li Z, Fan P, Deng M and Zeng C: The roles of RUNX3 in cervical cancer cells *in vitro*. Oncol Lett 15: 8729-8734, 2018.
22. Takeshima N, Yanoh K, Tabata T, Nagai K, Hirai Y and Hasumi K: Assessment of the revised international federation of gynecology and obstetrics staging for early invasive squamous cervical cancer. Gynecol Oncol 74: 165-169, 1999.

23. Livak KJ and Schmittgen TD: Analysis of relative gene expression data using real-time quantitative PCR and the 2(-Delta Delta C(T)) method. Methods 25: 402-408, 2001.
24. Yao T and Lin Z: MiR-21 is involved in cervical squamous cell tumorigenesis and regulates CCL20. Biochim Biophys Acta 1822: 248-260, 2012.
25. Long MJ, Wu FX, Li P, Liu M, Li X and Tang H: MicroRNA-10a targets CHL1 and promotes cell growth, migration and invasion in human cervical cancer cells. Cancer Lett 324: 186-196, 2012.
26. Qin W, Dong P, Ma C, Mitchelson K, Deng T, Zhang L, Sun Y, Feng X, Ding Y, Lu X, *et al*: MicroRNA-133b is a key promoter of cervical carcinoma development through the activation of the ERK and AKT1 pathways. Oncogene 31: 4067-4075, 2012.
27. Chen W, Tong K and Yu J: MicroRNA-130a is upregulated in colorectal cancer and promotes cell growth and motility by directly targeting forkhead box F2. Mol Med Rep 16: 5241-5248, 2017.
28. Yin S, Zhang Q, Wang Y, Li S and Hu R: MicroRNA-130a regulated by HPV18 E6 promotes proliferation and invasion of cervical cancer cells by targeting TIMP2. Exp Ther Med 17: 2837-2846, 2019.
29. Jiang H, Yu WW, Wang LL and Peng Y: miR-130a acts as a potential diagnostic biomarker and promotes gastric cancer migration, invasion and proliferation by targeting RUNX3. Oncol Rep 34: 1153-1161, 2015.
30. Chen J, Yan D, Wu W, Zhu J, Ye W and Shu Q: MicroRNA-130a promotes the metastasis and epithelial-mesenchymal transition of osteosarcoma by targeting PTEN. Oncol Rep 35: 3285-3292, 2016.
31. Sato K, Tomizawa Y, Iijima H, Saito R, Ishizuka T, Nakajima T and Mori M: Epigenetic inactivation of the RUNX3 gene in lung cancer. Oncol Rep 15: 129-135, 2006.
32. Zhang Z, Wang S, Wang M, Tong N, Fu G and Zhang Z: Genetic variants in RUNX3 and risk of bladder cancer: A haplotype-based analysis. Carcinogenesis 29: 1973-1978, 2008.
33. Lai KW, Koh KX, Loh M, Tada K, Subramaniam MM, Lim XY, Vaithilingam A, Salto-Tellez M, Iacopetta B, Ito Y, *et al*: MicroRNA-130b regulates the tumour suppressor RUNX3 in gastric cancer. Eur J Cancer 46: 1456-1463, 2010.
34. Gao QQ, Zhou B, Yu XZ, Zhang Z, Wang YY, Song YP, Zhang L, Luo H and Xi MR: Transcriptome changes induced by RUNX3 in cervical cancer cells *in vitro*. Oncol Lett 19: 651-662, 2010.
35. Cortez CC, Liang G, Van Rietschoten A, Jia L, Tsai YC, Egger G and Jones PA: RUNX3: Promoter 1 methylation status. Cancer Res 66 (8 Supp): S372, 2006.
36. Kim TY, Lee HJ, Hwang KS, Lee M, Kim JW, Bang YJ and Kang GH: Methylation of RUNX3 in various types of human cancers and premalignant stages of gastric carcinoma. Lab Invest 84: 479-484, 2004.
37. Park WS, Cho YG, Kim CJ, Song JH, Lee YS, Kim SY, Nam SW, Lee SH, Yoo NJ and Lee JY: Hypermethylation of the RUNX3 gene in hepatocellular carcinoma. Exp Mol Med 37: 276-281, 2005.
38. Li QL, Kim HR, Kim WJ, Choi JK, Lee YH, Kim HM, Li LS, Kim H, Chang J, Ito Y, *et al*: Transcriptional silencing of the RUNX3 gene by CpG hypermethylation is associated with lung cancer. Biochem Biophys Res Commun 314: 223-228, 2004.